Supplement of Eur. J. Mineral., 37, 455–482, 2025
https://doi.org/10.5194/ejm-37-455-2025-supplement

European Journal of Mineralogy
Open Access

Supplement of

Garnet growth across the quartz–coesite transition in metapelites: equilibrium vs. kinetics

Paola Manzotti et al.

Correspondence to: Paola Manzotti (paola.manzotti@geo.su.se)

Laboratory		
Microsonde Ouest, Brest (France)		
Instrument		
Cameca SX100 equipped with 5 WDS spectrometers		
Operating conditions for spot analyses		
15 kV accelerating voltage, 20 nA beam current, spot size = 1 µm. φ(ρZ) matrix correction was applied based on Pouchou and Pichoir (1985)		
Analysed mineral		
garnet, white mica		
Standard	**Counting time (peak)**	**Counting time (background)**
albite: Na, Si	**10**	**5**
orthoclase: K	10	5
corundum: Al	10	5
wollastonite: Ca	10	5
forsterite: Mg	10	5
$MnTiO_3$: Mn, Ti	30	15
andradite: Fe	10	5
Cr_2O_3: Cr	10	5
NiO: Ni	10	5
Operating conditions for X-ray maps		
15 kV accelerating voltage, 20 nA beam current, 0,1 s on 5µm pixel for garnet of Figs 3 and 6		
15 kV accelerating voltage, 100 nA beam current, 40 ms on 1µm pixel for garnet of Fig. 8		

Tab. S1 Operating conditions for microprobe analyses.

Mineral abbreviations	
ab	albite
alm	almandine
car	carpholite
chl	chlorite
coe	coesite
ctd	chloritoid
ep	epidote
g	garnet
gl	sodic amphibole
gph	graphite
grs	grossular
jd	jadeite
ky	kyanite
law	lawsonite
mu	muscovite
pa	paragonite
prp	pyrope
q	quartz
ru	rutile
spss	spessartine

Other symbols (mole/atomic proportions)		
X_{Mg}	Mg/(Fe + Mg)	for g, mu
alm	Fe^{2+}/(Fe^{2+} + Mg + Ca + Mn)	
spss	Mn/(Fe^{2+} + Mg + Ca + Mn)	
prp	Mg/(Fe^{2+} + Mg + Ca + Mn)	
grs	Ca/(Fe^{2+} + Mg + Ca + Mn)	
X_{Na}	Na/(Na + K)	for mu
a.p.f.u.	atom per formula unit	
wt%	weight per cent	
mol%	mole per cent	
vol %	volume per cent	

Tab. S2 Mineral abbreviations and other symbols used in this study.

Mineral	**g**	**g**	**g**	**g**	**g**	**g**	**g**	**g**	**g**	**mu**	**mu**	**mu**	**mu**	**pa**	**pa**
Zone	rim	rim	rim	outer core	outer core	outer core	inner core	inner core	inner core	S_{1-2} core	S_{1-2} core	S_{1-2} rim	S_{1-2} rim	S_{1-2}	S_{1-2}
Analysis	108	1	106	93	71	69	40	66	51	8	7	27	36	40	13
SiO_2	36.93	37.34	36.85	37.44	36.65	36.77	37.08	37.10	36.90	52.89	53.04	49.99	49.93	47.75	47.37
TiO_2	0.10	0.06	0.09	0.01	0.03	0.05	0.08	0.07	0.03	0.15	0.13	0.27	0.28	0.06	0.06
Cr_2O_3	<0.01	<0.01	<0.01	<0.01	0.01	0.01	<0.01	<0.01	<0.01	<0.01	<0.01	0.01	<0.01	<0.01	<0.01
NiO	0.02	0.04	<0.01	<0.01	0.03	0.01	0.02	<0.01	<0.01	0.09	<0.01	<0.01	0.06	0.01	0.05
Al_2O_3	20.98	21.01	20.95	21.29	21.03	21.15	21.07	21.26	20.98	25.15	25.72	28.93	28.02	38.94	39.57
FeO	34.87	35.24	36.97	36.91	38.08	36.89	36.66	35.85	36.06	2.30	2.05	3.14	3.45	0.33	0.19
MnO	0.22	0.42	0.28	0.63	1.45	2.03	1.66	2.19	2.23	<0.01	<0.01	<0.01	0.03	<0.01	<0.01
MgO	0.82	0.86	1.22	2.77	1.43	1.65	1.69	1.74	1.68	4.32	4.45	2.47	2.70	0.37	0.21
CaO	6.63	5.92	4.30	2.20	1.98	2.13	2.33	2.52	2.63	<0.01	0.05	<0.01	<0.01	0.05	0.04
Na_2O	0.03	0.03	0.04	0.04	0.04	0.04	0.07	0.06	0.08	0.15	0.05	0.41	0.41	7.04	7.46
K_2O	<0.01	<0.01	<0.01	0.01	0.01	<0.01	<0.01	<0.01	<0.01	11.32	11.02	10.78	10.54	1.37	0.83
Total	100.60	100.92	100.70	101.30	100.74	100.73	100.66	100.79	100.59	96.37	96.51	96.00	95.42	95.92	95.78
Oxygen-equivalents	12	12	12	12	12	12	12	12	12	11	11	11	11	11	11
Si	2.97	3.00	2.97	2.98	2.96	2.97	2.99	2.98	2.98	3.50	3.49	3.33	3.35	3.04	3.01
Ti	0.01	0.00	0.01	0.00	0.00	0.00	0.00	0.00	0.00	0.01	0.01	0.01	0.01	0.00	0.00
Cr	0.00	0.00	0.00	0.00	0.00	0.00	0.00	0.00	0.00	0.00	0.00	0.00	0.00	0.00	0.00
Ni	0.00	0.00	0.00	0.00	0.00	0.00	0.00	0.00	0.00	0.01	0.00	0.00	0.00	0.00	0.00
Al	1.99	1.99	1.99	2.00	2.00	2.01	2.00	2.00	1.99	1.96	1.99	2.27	2.22	2.92	2.96
Fe^{3+}	0.07	0.02	0.07	0.05	0.07	0.05	0.02	0.02	0.06	0.00	0.00	0.00	0.00	0.00	0.00
Fe^{2+}	2.28	2.35	2.43	2.41	2.50	2.44	2.46	2.40	2.37	0.13	0.11	0.17	0.19	0.02	0.01
Mn	0.01	0.03	0.02	0.04	0.10	0.14	0.11	0.15	0.15	0.00	0.00	0.00	0.00	0.00	0.00
Mg	0.10	0.10	0.15	0.33	0.17	0.20	0.20	0.21	0.20	0.43	0.44	0.25	0.27	0.04	0.02
Ca	0.57	0.51	0.37	0.19	0.17	0.18	0.20	0.22	0.23	0.00	0.00	0.00	0.00	0.00	0.00
Na	0.00	0.00	0.01	0.00	0.01	0.00	0.01	0.01	0.01	0.02	0.01	0.05	0.05	0.87	0.92
K	0.00	0.00	0.00	0.00	0.00	0.00	0.00	0.00	0.00	0.96	0.92	0.92	0.90	0.11	0.07
Total	8.00	8.00	8.02	8.00	7.98	7.99	7.99	7.99	7.99	7.02	6.97	7.00	6.99	7.00	6.99
X_{Mg}	0.04	0.04	0.06	0.12	0.06	0.08	0.08	0.08	0.08	0.77	0.80	0.60	0.59	0.67	0.67
alm	77	79	82	81	85	82	83	81	80						
prp	3	3	5	11	6	7	7	7	7						
grs	19	17	12	6	6	6	7	7	8						
spss	0	1	1	1	3	5	4	5	5						

Tab. S3 Representative mineral analyses and formulas of garnet, muscovite, and paragonite in the garnet-chloritoid micaschist MU23 from the Muret Unit.

Mineral	**g**	**g**	**g**	**g**	**g**	**g**	**mu**	**mu**	**mu**	**mu**	**pa**	**pa**
Zone	outer core	outer core	outer core	inner core	inner core	inner core	S_{1-2} core	S_{1-2} core	S_{1-2} rim	S_{1-2} rim	S_{1-2}	S_{1-2}
Analysis	6	118	115	61	66	71	71	10	62	22	2	6
SiO_2	36.83	36.99	36.91	36.21	36.59	36.50	52.86	51.66	49.68	49.81	47.29	47.26
TiO_2	0.08	0.02	0.02	0.04	0.02	0.02	0.12	0.16	0.30	0.17	0.08	0.09
Cr_2O_3	<0.01	<0.01	<0.01	<0.01	<0.01	<0.01	0.01	0.03	0.01	0.03	0.01	<0.01
NiO	<0.01	<0.01	<0.01	<0.01	0.05	<0.01	<0.01	<0.01	<0.01	0.00	0.06	<0.01
Al_2O_3	21.08	21.02	21.00	20.94	20.93	20.80	25.10	27.44	30.12	28.98	39.70	39.48
FeO	36.77	36.21	37.13	35.57	34.64	35.28	2.79	2.73	3.18	3.40	0.37	0.44
MnO	1.60	0.89	1.16	4.40	4.17	3.99	<0.01	<0.01	<0.01	<0.01	<0.01	<0.01
MgO	2.21	2.31	2.32	1.23	1.55	1.52	4.23	3.32	2.43	2.32	0.31	0.27
CaO	2.04	2.76	2.25	1.82	2.19	1.97	<0.01	0.02	<0.01	0.01	0.05	0.03
Na_2O	0.05	0.02	0.03	<0.01	0.06	0.03	0.16	0.20	0.58	0.53	6.91	6.84
K_2O	<0.01	<0.01	<0.01	0.01	0.01	<0.01	11.26	10.45	9.87	10.36	1.12	1.07
Total	100.66	100.22	100.82	100.22	100.21	100.11	96.53	96.01	96.17	95.61	95.84	95.48
Oxygen-equivalents	12	12	12	12	12	12	11	11	11	11	11	11
Si	2.96	2.98	2.96	2.96	2.97	2.97	3.50	3.42	3.29	3.33	3.00	3.01
Ti	0.00	0.00	0.00	0.00	0.00	0.00	0.01	0.01	0.01	0.01	0.00	0.00
Cr	0.00	0.00	0.00	0.00	0.00	0.00	0.00	0.00	0.00	0.00	0.00	0.00
Ni	0.00	0.00	0.00	0.00	0.00	0.00	0.00	0.00	0.00	0.00	0.00	0.00
Al	2.00	2.00	1.99	2.01	2.00	1.99	1.96	2.14	2.35	2.28	2.97	2.97
Fe^{3+}	0.07	0.04	0.09	0.08	0.07	0.07	0.00	0.00	0.00	0.00	0.00	0.00
Fe^{2+}	2.40	2.40	2.41	2.34	2.28	2.33	0.15	0.15	0.18	0.19	0.02	0.02
Mn	0.11	0.06	0.08	0.30	0.29	0.27	0.00	0.00	0.00	0.00	0.00	0.00
Mg	0.26	0.28	0.28	0.15	0.19	0.18	0.42	0.33	0.24	0.23	0.03	0.03
Ca	0.18	0.24	0.19	0.16	0.19	0.17	0.00	0.00	0.00	0.00	0.00	0.00
Na	0.01	0.00	0.00	0.00	0.01	0.01	0.02	0.03	0.07	0.07	0.85	0.85
K	0.00	0.00	0.00	0.00	0.00	0.00	0.95	0.88	0.83	0.88	0.09	0.09
Total	7.99	8.00	8.00	8.00	8.00	7.99	7.01	6.96	6.97	6.99	6.96	6.97
X_{Mg}	0.10	0.10	0.10	0.06	0.08	0.07	0.74	0.69	0.57	0.55	0.60	0.60
alm	81	81	81	79	77	79						
prp	9	9	9	5	6	6						
grs	6	8	6	5	6	6						
spss	4	2	3	10	10	9						

Tab. S4 Representative mineral analyses and formulas of garnet, muscovite, and paragonite in the garnet-chloritoid micaschist MU7 from the Muret Unit.

Mineral	g	g	g	g	g	g	g	g	g	mu	mu	mu	mu	pa	pa
Zone	rim	rim	rim	outer core	outer core	outer core	inner core	inner core	inner core	core	core	rim	rim	core	core
Analysis	354	356	361	364	365	370	305	309	313	82	61	78	85	1	69
SiO_2	37.18	37.06	37.03	37.26	36.89	36.98	36.71	36.93	36.86	52.64	51.90	49.55	48.65	46.37	46.27
TiO_2	<0.01	0.01	<0.01	<0.01	<0.01	<0.01	<0.01	0.01	<0.01	0.11	0.11	0.26	0.31	0.01	0.02
Cr_2O_3	<0.01	<0.01	<0.01	0.01	0.03	<0.01	0.01	<0.01	0.03	<0.01	0.01	<0.01	<0.01	0.02	0.01
NiO	<0.01	<0.01	<0.01	<0.01	<0.01	<0.01	<0.01	0.02	<0.01	<0.01	<0.01	<0.01	<0.01	<0.01	<0.01
Al_2O_3	21.08	21.10	21.26	21.15	21.17	21.16	20.91	20.97	21.01	25.00	26.89	30.15	30.83	41.51	41.37
FeO	31.75	31.64	34.22	34.87	35.41	36.05	34.75	34.95	35.23	2.90	2.10	3.15	3.38	0.32	0.27
MnO	0.62	0.42	0.70	0.76	0.84	0.88	4.57	4.33	4.10	0.02	0.05	<0.01	0.03	0.03	<0.01
MgO	0.70	0.78	2.03	2.48	2.47	2.40	1.57	1.61	1.66	4.22	4.13	2.60	2.31	0.04	0.15
CaO	8.54	9.14	5.19	3.67	3.37	3.06	1.76	1.61	1.75	<0.01	<0.01	<0.01	<0.01	0.07	0.08
Na_2O	<0.01	<0.01	<0.01	<0.01	<0.01	<0.01	<0.01	<0.01	<0.01	0.02	0.10	0.45	0.41	7.64	7.17
K_2O	<0.01	<0.01	<0.01	<0.01	<0.01	<0.01	<0.01	<0.01	<0.01	10.79	11.16	10.48	10.18	0.44	0.71
Total	99.87	100.15	100.43	100.20	100.18	100.53	100.28	100.43	100.64	95.70	96.45	96.64	96.10	96.45	96.04
Oxygen-equivalents	12	12	12	12	12	12	12	12	12	11	11	11	11	11	11
Si	3.00	2.97	2.97	2.99	2.97	2.97	2.98	2.99	2.98	3.50	3.42	3.27	3.23	2.93	2.93
Ti	0.00	0.00	0.00	0.00	0.00	0.00	0.00	0.00	0.00	0.01	0.01	0.01	0.02	0.00	0.00
Cr	0.00	0.00	0.00	0.00	0.00	0.00	0.00	0.00	0.00	0.00	0.00	0.00	0.00	0.00	0.00
Ni	0.00	0.00	0.00	0.00	0.00	0.00	0.00	0.00	0.00	0.00	0.00	0.00	0.00	0.00	0.00
Al	2.00	2.00	2.01	2.00	2.01	2.00	2.00	2.00	2.00	1.96	2.09	2.35	2.42	3.09	3.09
Fe^{3+}	0.01	0.06	0.06	0.01	0.06	0.06	0.04	0.01	0.03	0.00	0.00	0.00	0.00	0.00	0.00
Fe^{2+}	2.13	2.07	2.23	2.33	2.32	2.36	2.32	2.36	2.35	0.16	0.12	0.17	0.19	0.02	0.01
Mn	0.04	0.03	0.05	0.05	0.06	0.06	0.31	0.30	0.28	0.00	0.00	0.00	0.00	0.00	0.00
Mg	0.08	0.09	0.24	0.30	0.30	0.29	0.19	0.19	0.20	0.42	0.41	0.26	0.23	0.00	0.01
Ca	0.74	0.79	0.45	0.32	0.29	0.26	0.15	0.14	0.15	0.00	0.00	0.00	0.00	0.00	0.01
Na	0.00	0.00	0.00	0.00	0.00	0.00	0.00	0.00	0.00	0.00	0.01	0.06	0.05	0.93	0.88
K	0.00	0.00	0.00	0.00	0.00	0.00	0.00	0.00	0.00	0.92	0.94	0.88	0.86	0.04	0.06
Total	8.00	8.00	8.01	8.00	8.01	8.00	7.99	7.99	7.99	6.97	7.00	7.00	7.00	7.01	6.99
X_{Mg}	0.04	0.04	0.10	0.11	0.11	0.11	0.08	0.07	0.08	0.72	0.77	0.60	0.55	0.00	0.50
alm	71	69	75	78	78	79	78	79	79						
prp	3	3	8	10	10	10	6	6	7						
grs	25	27	15	11	10	9	5	5	5						
spss	1	1	2	2	2	2	10	10	9						

Tab. S5 Representative mineral analyses and formulas of garnet, muscovite, and paragonite in the garnet-chloritoid micaschist SE8 from the Serre Unit.

Unit	Sample	Comment	SiO_2	Al_2O_3	Fe_2O_3	MnO	MgO	CaO	Na_2O	K_2O	TiO_2	P_2O_5
Muret Unit	MU23	unfractionated	64.79	18.85	7.35	0.04	2.10	0.42	2.40	3.05	1.00	0.02
		fractionated for g inner core	64.05	18.43	6.56	0.01	2.07	0.36	2.40	3.05	1.00	0.02
		fractionated for g outer core	62.93	17.80	5.35	0.01	1.99	0.29	2.40	3.05	1.00	0.02
	MU7	unfractionated	65.75	18.86	7.01	0.08	2.00	0.33	1.00	3.88	0.92	0.10
		fractionated for g inner core	65.02	18.44	6.24	0.01	1.97	0.29	1.00	3.88	0.92	0.10
Serre Unit	MU8	unfractionated	60.88	21.74	8.03	0.25	1.96	0.67	1.35	5.00	0.80	0.14
		fractionated for g inner core	60.51	21.53	7.64	0.21	1.94	0.65	1.35	4.05	0.80	0.14
		fractionated for g outer core	59.96	21.21	7.03	0.19	1.91	0.62	1.35	4.05	0.80	0.14
Muret Unit	GM1	Nosenzo et al., 2023	62.50	21.48	5.88	0.02	2.71	0.22	0.86	5.03	1.17	0.14
	GM2		53.07	25.12	8.56	0.05	4.35	0.08	1.35	5.92	1.38	0.00
	GM13		60.12	19.14	8.53	0.02	2.96	0.59	1.44	5.07	0.71	0.00

Tab. S6 Whole-rock compositions (wt%) used for thermodynamic modelling.

Standard spot	**128** measured (cm^{-1})	**206** measured (cm^{-1})	**464** measured (cm^{-1})	**ω1**	**ω2**
Spot 1	128.29	206.89	464.34	257.44	78.61
Spot 2	128.23	206.79	464.31	257.52	78.56
Average	128.26	206.84	464.32	257.48	78.58
St Dev	0.04	0.07	0.02	0.05	0.04

Tab. S7 Data of Raman shift of α-quartz : $\varpi_1 = \nu_{464} - \nu_{206}$; $\varpi_2 = \nu_{206} - \nu_{128}$

Software		
Theriak-Domino (de Capitani and Brown 1987; de Capitani and Petrakakis 2010)		
Thermodynamic dataset		
Holland and Powell 2011 version ds6.2		
Solution models (minerals)		
	Mineral	**Solution model**
Orthosilicates	Garnet	White et al. 2014a, 2014b
	Kyanite	pure
	Chloritoid	White et al. 2014a, 2014b
	Staurolite	White et al. 2002; Holland and Powell 2003
Disilicates	Epidote	Holland and Powell 2011
	Lawsonite	pure
Chain silicates	Clinopyroxene	Green et al. 2016
	Amphibole	Green et al. 2016
	Carpholite	Wei and Powell 2004, ideal
Sheet silicates	White mica	White et al. 2014a, 2014b
	Biotite	White et al. 2014a, 2014b
	Chlorite	White et al. 2014a, 2014b
Framework silicates	Plagioclase	Holland and Powell 2003
	Quartz/Coesite	pure
Oxydes	Rutile	pure
	Ilmenite	White et al. 2000
	Magnetite	White et al. 2002
Solution models (fluid)		
	H_2O	pure

Tab. S8 Phases and activity composition models considered in the thermodynamic calculations.

Section S1
Garnet fractionation

Very high-resolution plane-polarised photomicrographs of the entire thin sections have been acquired with a Nikon Super Coolscan 9000 ED (Stockholm University). The modal amount of garnet was estimated in each thin section, measuring the garnet surface with respect to the surface of the entire thin section using a graphic software (ImageJ open-source; Rasband, 1997). The modal amount of garnet inner and outer cores has been estimated on the basis of backscattered images and X-ray maps using the software ImageJ. X-ray maps were acquired on selected garnet porphyroblasts. Representative chemical compositions of garnet inner and outer cores were subtracted from the measured bulk composition in proportion to the modal amount of the garnet inner and outer cores. The relative proportion of garnet rims with respect to garnet inner and outer cores has been also estimated by image analysis (on backscattered images of garnet porphyroblasts) using the software ImageJ. Because there is no evidence that the andradite component is concentrated in the garnet core with respect to the garnet rim the ratio FeO/Fe_2O_3 in the bulk is considered constant.

Section S2
Raman spectroscopy on carbonaceous material (RSCM) method

Regional metamorphic processes produce a gradual transformation of the organic matter present in rocks to CM (carbonaceous material). The temperature of regional metamorphism controls the degree of graphitization (Beyssac et al. 2002, 2003). Because graphitization is considered as an irreversible process, the *T* estimates are not affected by metamorphic reactions associated with retrogression. Thus, this graphitization process allows us to estimate the peak *T* reached by CM-bearing samples.

Carbonaceous material was analysed in three samples. Raman spectra of CM were obtained at the Laboratoire Magmas et Volcans (Clermont-Ferrand, France) using a Renishaw inVia confocal micro-spectrometer, equipped with a 532 nm diode-pulsed solid state laser. Because RSCM can be affected by several analytical mismatches, we followed closely the analytical procedures described by Beyssac et al. (2002, 2003). Measurements were carried out on polished thin sections using a grating of 2400 grooves/mm, a 20 μm slit aperture (high confocality setting), a ×100 microscope objective, and 1-5 mW laser power on the sample surface. The laser was generally focused at 5-15 μm depth to analyse graphite that was located below different minerals and not exposed at the surface. Each analysis consisted of 6 or 10 accumulations of 20 seconds each in the ~900-2000 cm^{-1} wavenumber range, containing the two principal vibrations of graphite. On each sample, we measured more than 20 different grains of graphite. The spectra were processed using the WiRE^{TM} 4.4 software: first, they were truncated, then a linear baseline correction was applied in the 1200-1800 cm^{-1} spectral range, and finally curve fitting was performed. Three bands (corresponding to G, D1, and D2 components, respectively at ~1580, ~1350, and ~1620 cm^{-1}) were necessary to fit the graphite spectrum. The degree of organization of CM is quantified by the relative area of the G, D1, and D2 components in the Raman spectrum of CM, and expressed as an R2 ratio equal to D1⁄(G + D1 + D2) (Beyssac et al. 2002, 2003).

Unit	Sample	Lithology	n	R2	T (°C)	SD	Confidence
Chasteiran	CH11*	garnet-chloritoid micaschist	19	0.25-0.40	483	17	5
Muret	MU2110	garnet-glaucophane micaschist	22	0.11-0.29	547	22	9
	MU7	garnet-chloritoid micaschist	23	0.20-0.38	516	22	9
Serre	SE8	garnet-chloritoid micaschist	22	0.12-0.46	500	48	20

Tab. S9 RSCM results (number of Raman spectra, R2 ratio, RSCM temperature, standard deviation, and confidence) from the studied samples. * Manzotti et al. (2022)

Reference	SiO_2	Al_2O_3	Fe_2O_3	MnO	MgO	CaO	Na_2O	K_2O	TiO_2
Forshaw & Pattison 2023	64.13	19.63	7.61	0.08	2.41	0.65	1.38	3.95	0.91
Variation in CaO content	64.13	19.63	7.61	0.08	2.41	1.50	1.38	3.95	0.91
	64.13	19.63	7.61	0.08	2.41	2.50	1.38	3.95	0.91
Variation in Mg/(Mg+Fe) ratio	64.13	19.63	8.92	0.08	1.10	0.65	1.38	3.95	0.91
	64.13	19.63	5.71	0.08	4.31	0.65	1.38	3.95	0.91

Tab. S10 Whole-rock compositions (wt%) used for thermodynamic modelling (Figs 15, 16 and S20).

SAMPLE MU23 (MANIGLIA LOCALITY)

Fig. S1 Photomicrograph (plane-polarised light) of the thin section MU23a (sample MU23).

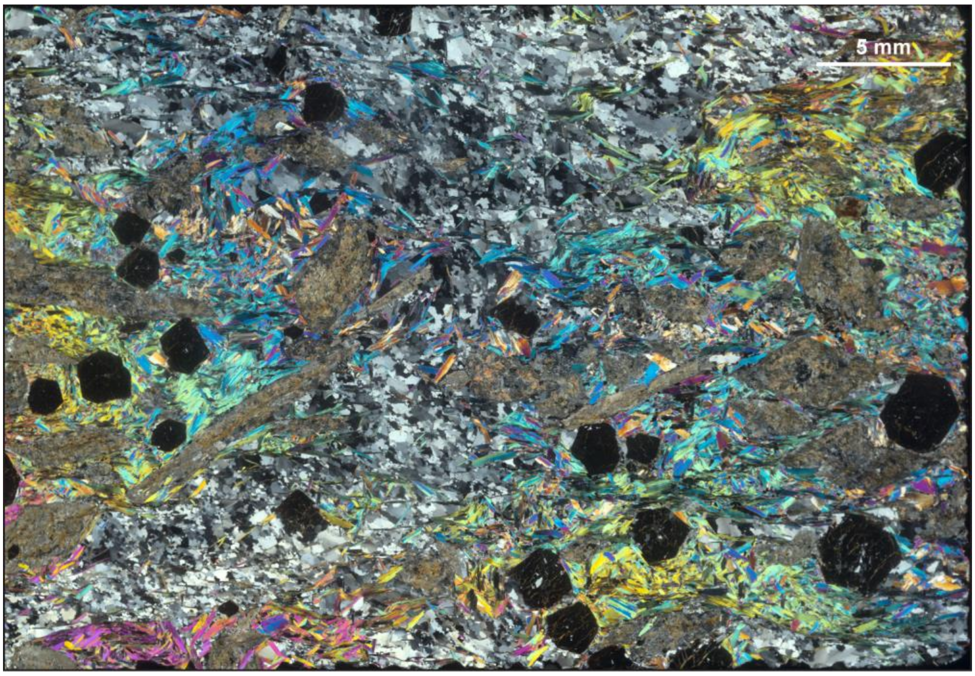

Fig. S2 Photomicrograph (cross-polarised light) of the thin section MU23a (sample MU23).

Fig. S3 Photomicrograph (plane-polarised light) of the thin section MU23b (sample MU23).

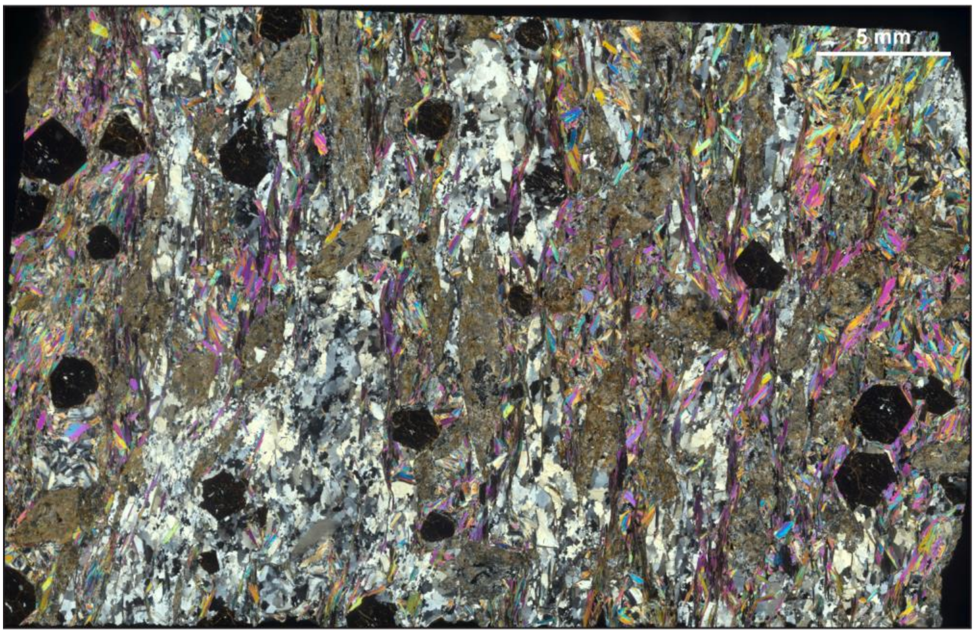

Fig. S4 Photomicrograph (cross-polarised light) of the thin section MU23b (sample MU23).

SAMPLE MU217 (MANIGLIA LOCALITY)

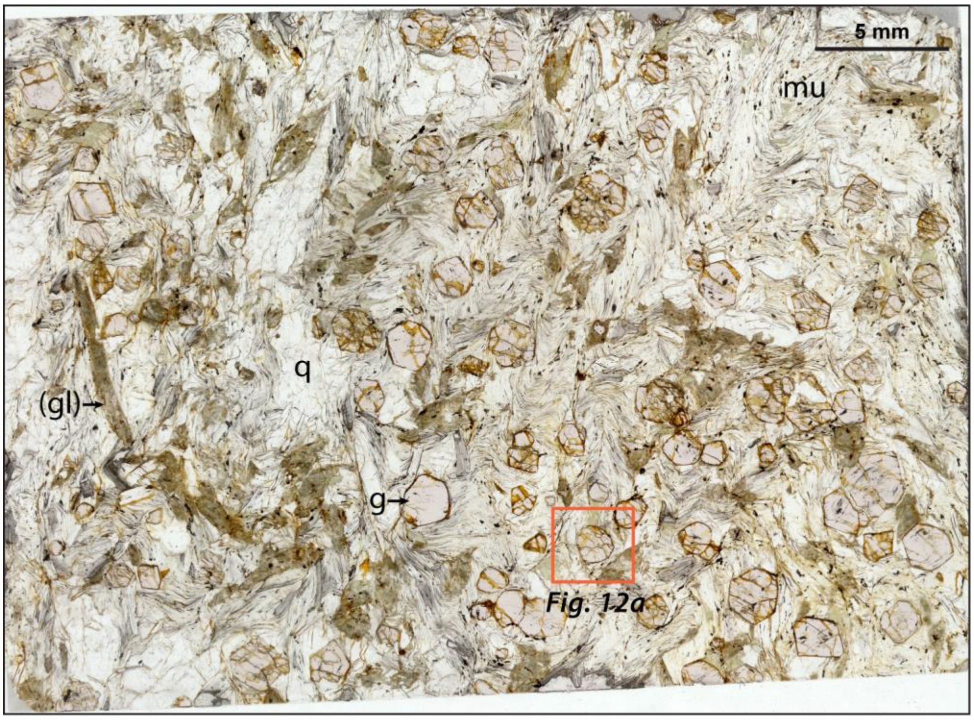

Fig. S5 Photomicrograph (plane-polarised light) of the thin section MU217 (sample MU217). The orange square refers to the location of a garnet containing a coesite inclusion (see Fig. 12a for a closer view).

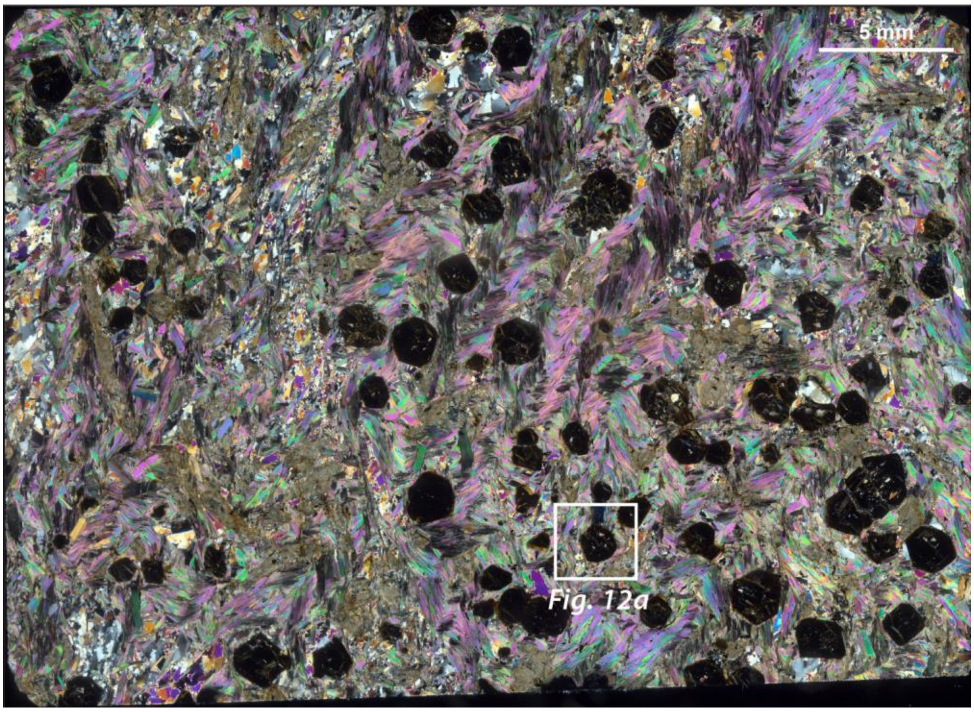

Fig. S6 Photomicrograph (cross-polarised light) of the thin section MU217 (sample MU217). The white square refers to the location of a garnet containing a coesite inclusion (see Fig. 12a for a closer view).

SAMPLE MU2110 (MANIGLIA LOCALITY)

Fig. S7 Photomicrograph (plane-polarised light) of the thin section MU2110 (sample MU2110).

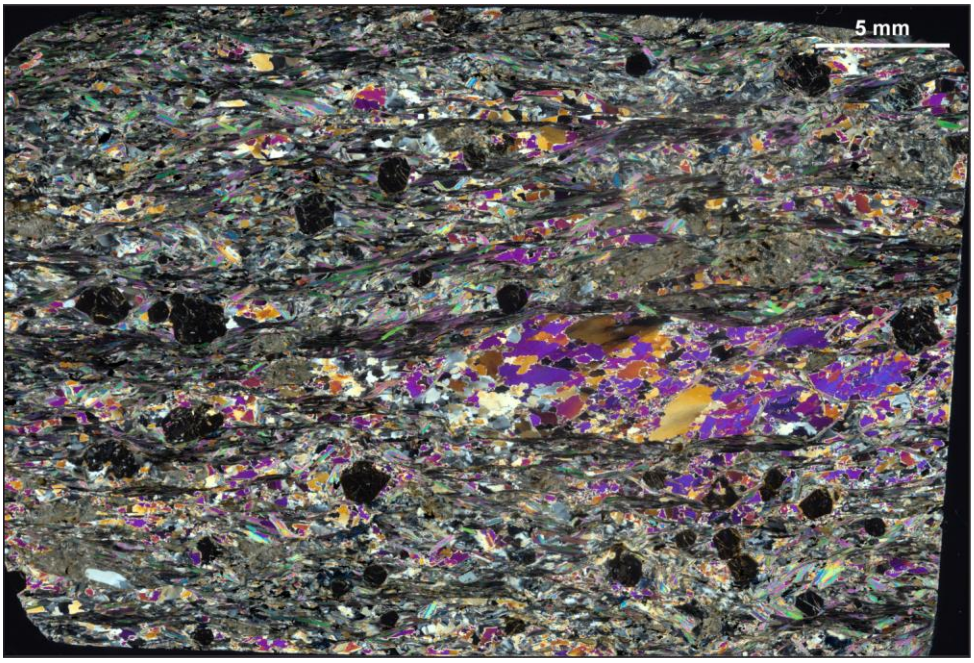

Fig. S8 Photomicrograph (cross-polarised light) of the thin section MU2110 (sample MU2110).

SAMPLE MU7 (FONTANE LOCALITY)

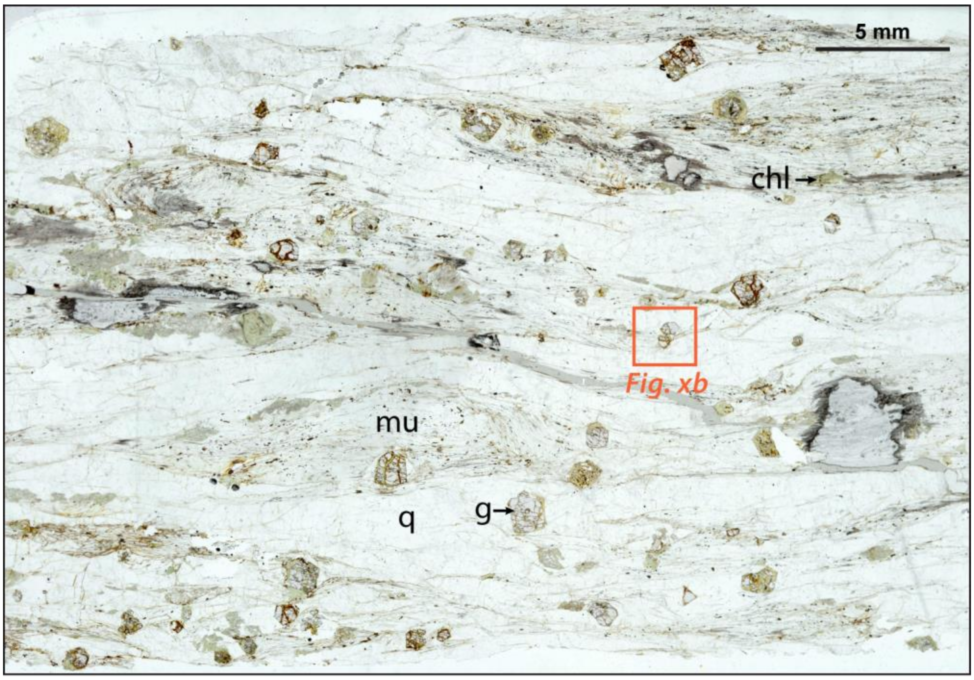

Fig. S9 Photomicrograph (plane-polarised light) of the thin section MU7a (sample MU7). The orange square refers to the location of a garnet containing a coesite inclusion (see Fig. 12b for a closer view).

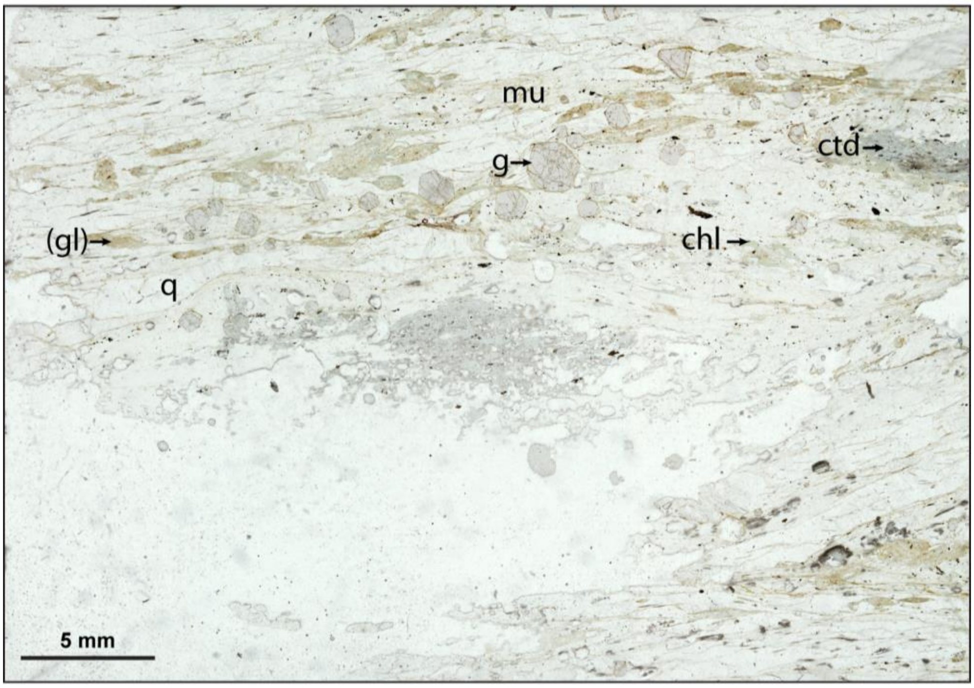

Fig. S10 Photomicrograph (plane-polarised light) of the thin section MU7b (sample MU7).

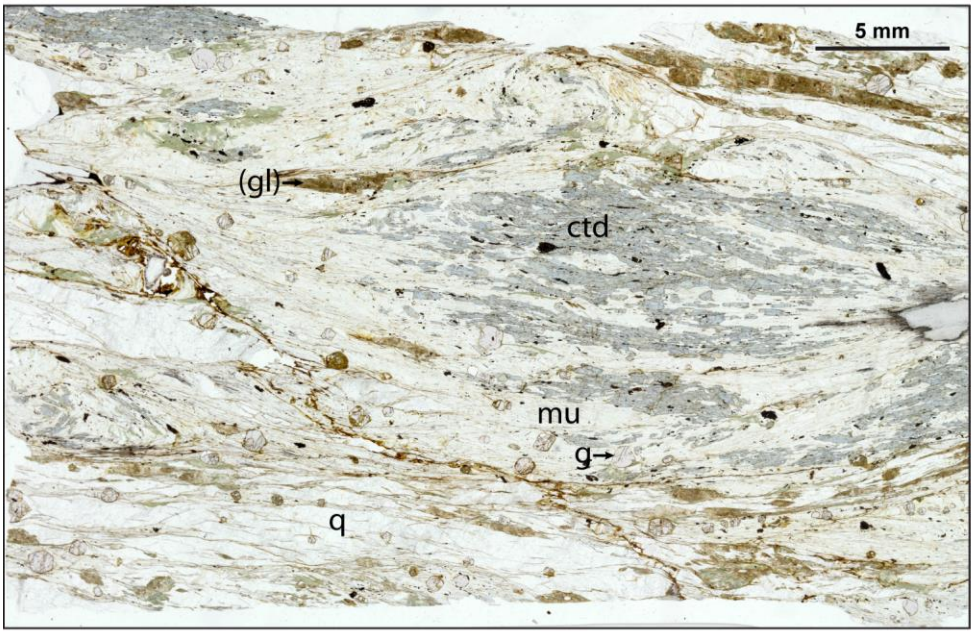

Fig. S11 Photomicrograph (plane-polarised light) of the thin section MU7c (sample MU7).

SAMPLE SE8 (COL CLAPIER LOCALITY)

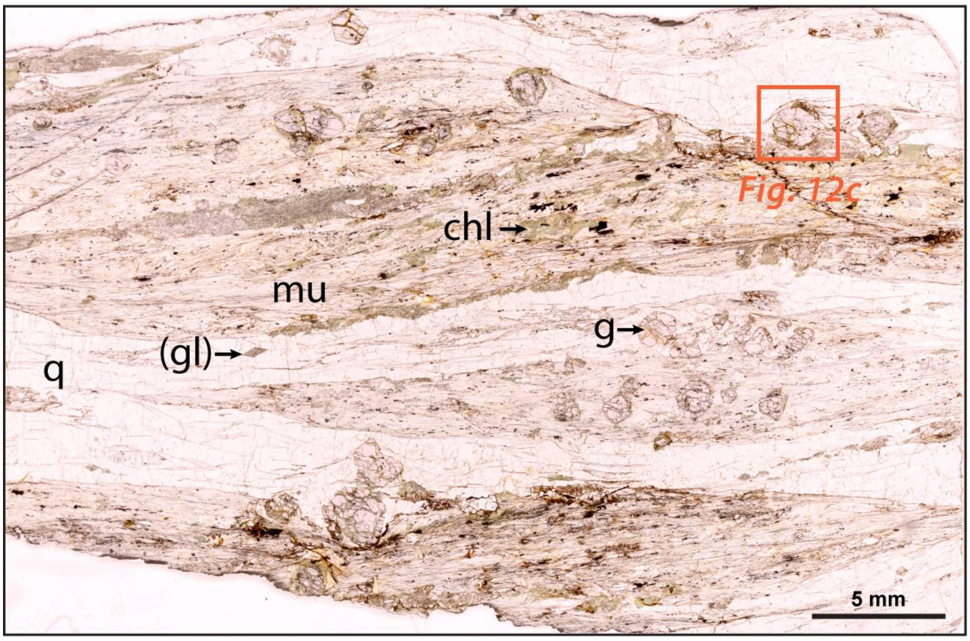

Fig. S12 Photomicrograph (plane-polarised light) of the thin section SE8a (sample SE8). The orange square refers to the location of a garnet containing a coesite inclusion (see Fig. 12c for a closer view).

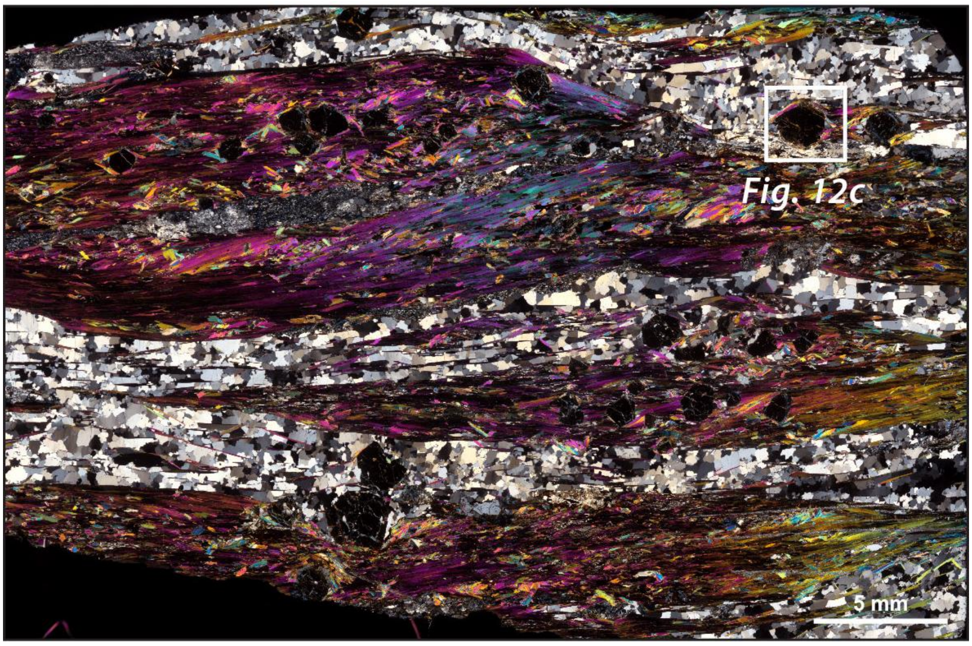

Fig. S13 Photomicrograph (cross-polarised light) of the thin section SE8a (sample SE8). The white square refers to the location of a garnet containing a coesite inclusion (see Fig. 12c for a closer view).

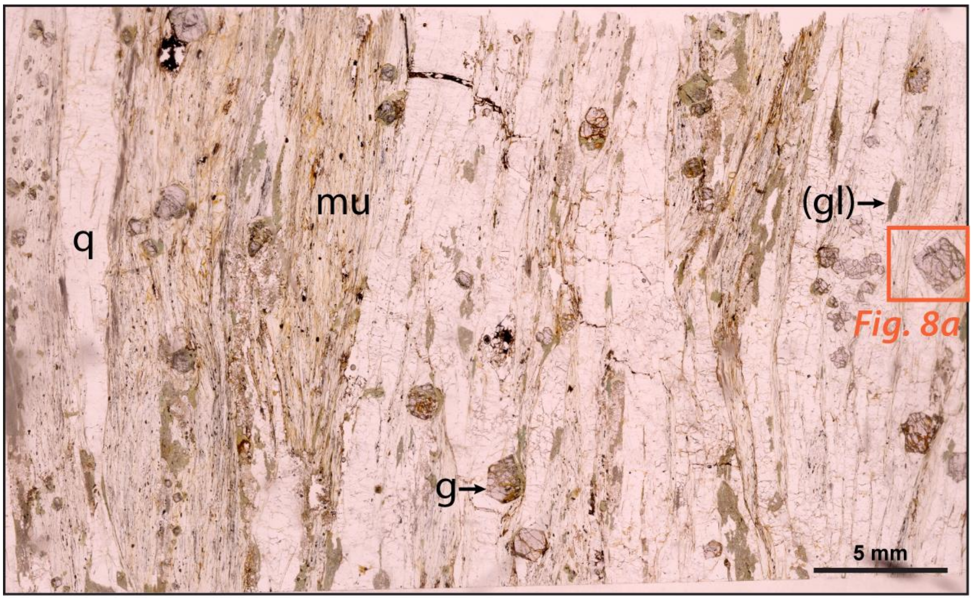

Fig. S14 Photomicrograph (plane-polarised light) of the thin section SE8b (sample SE8). The orange square refers to the location of a garnet containing a coesite inclusion (see Fig. 8a for a closer view).

Fig. S15 Photomicrograph (cross-polarised light) of the thin section SE8b (sample SE8). The white square refers to the location of a garnet containing a coesite inclusion (see Fig. 8a for a closer view).

Fig. S16 Photomicrograph (plane-polarised light) of the thin section SE8c (sample SE8).

Fig. S17 Photomicrograph (cross-polarised light) of the thin section SE8c (sample SE8).

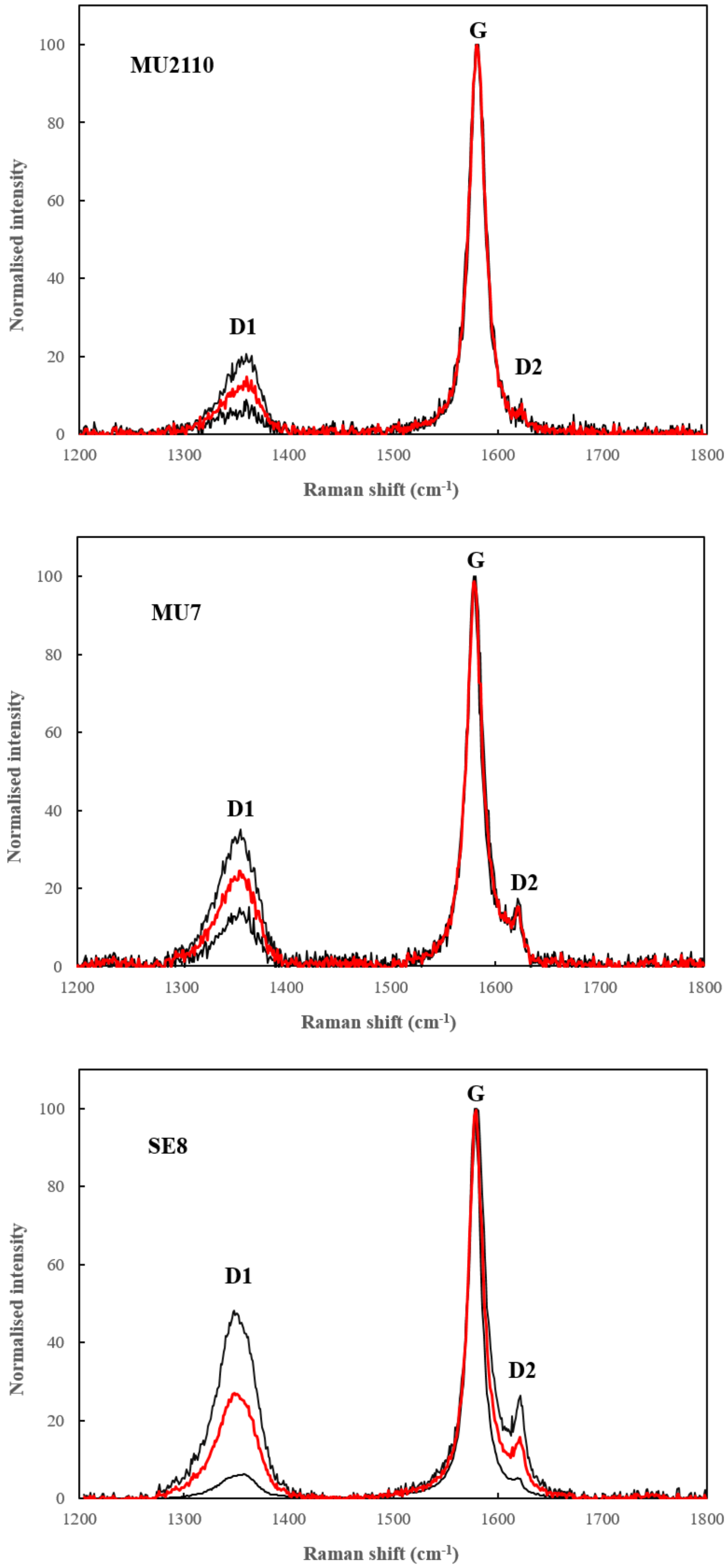

Fig. S18: Representative Raman spectra of carbonaceous material from samples MU2110, MU7 and SE8. For each sample, the spectra corresponding to the maximum, minimum and intermediate temperatures are shown.

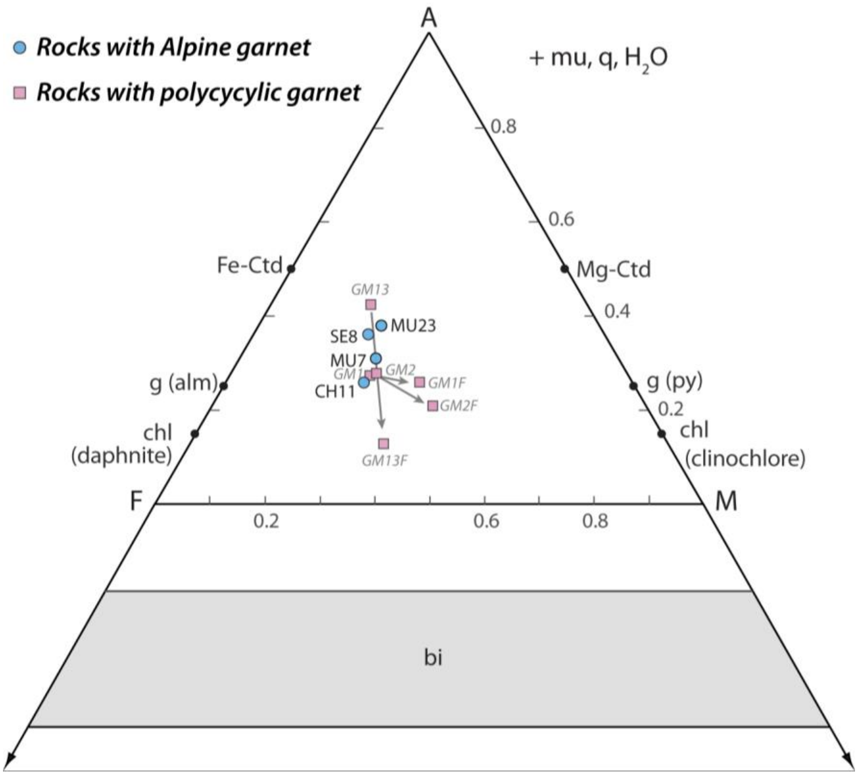

Fig. S19: AFM diagram showing the bulk-rock compositions of the studied samples from the Muret and Serre Units projected from muscovite, quartz, and H_2O. Compositions of the metapelites from the Muret and Chasteiran Units studied by Nosenzo et al. (2023) and Manzotti et al. (2022), respectively are also plotted. GM1F, GM2F, GM13F are the bulk rock compositions after garnet fractionation, used for thermodynamic modelling. The grey arrows indicate the change of composition after garnet fractionation.

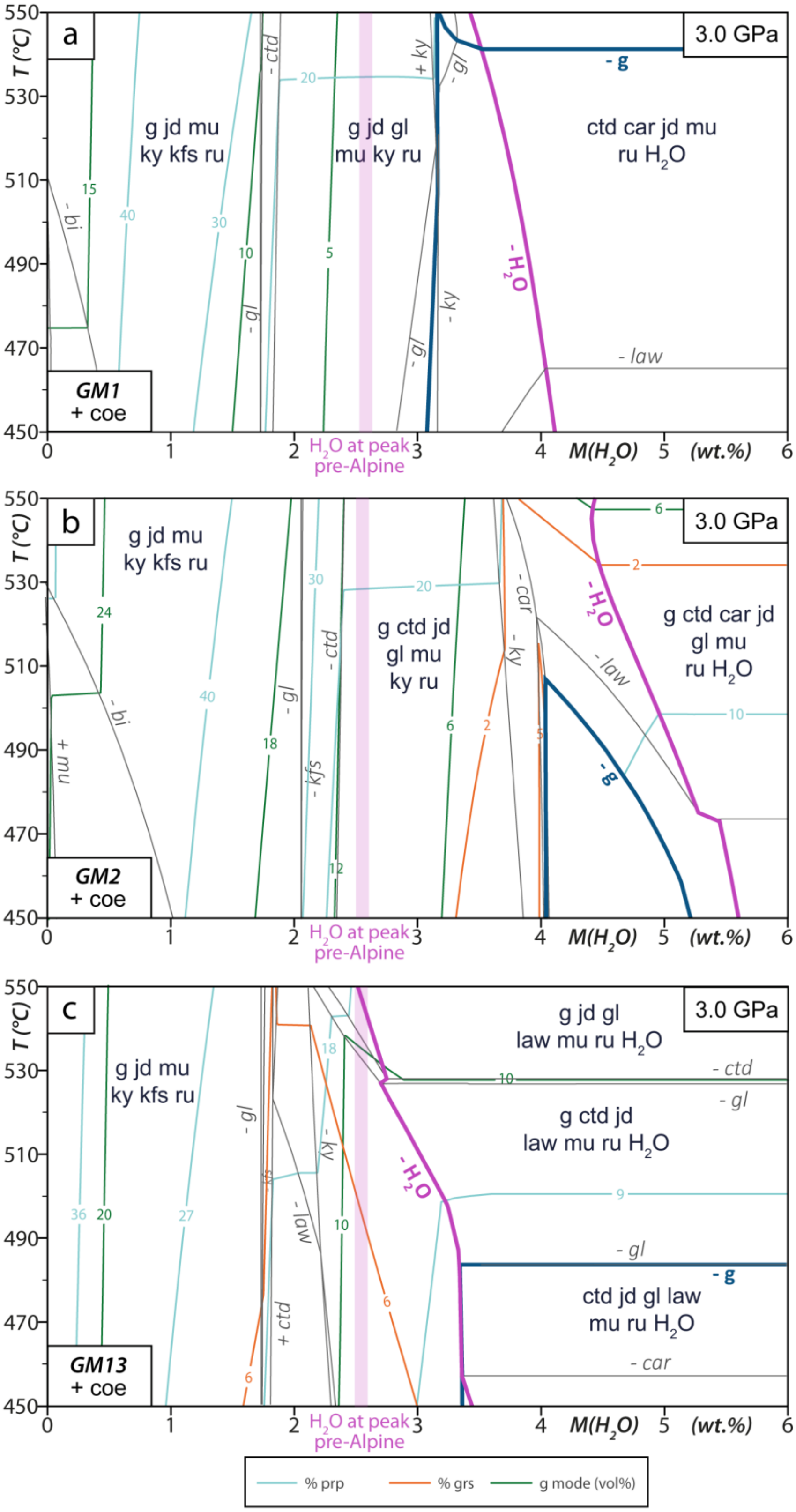

Fig. S20: *T–M(H_2O)* pseudosections calculated at 3.0 GPa for the Alpine evolution of the polycyclic rocks. Samples GM1 (a), GM2 (b), and GM13 (c). Some fields are not labelled for the safe of clarity; their assemblages can be deduced from the assemblages in adjacent fields. The grossular content in (a) (sample GM1) is equal to 0 in the entire investigated *T–M(H_2O)* space. Pink vertical bands indicate the calculated mineral-bound H_2O at peak pre-Alpine conditions with the addition of 1 vol% of free H_2O phase (see Nosenzo et al., 2023 for a complete discussion about the H_2O content in the polycyclic rocks from the northern Dora-Maira Massif).

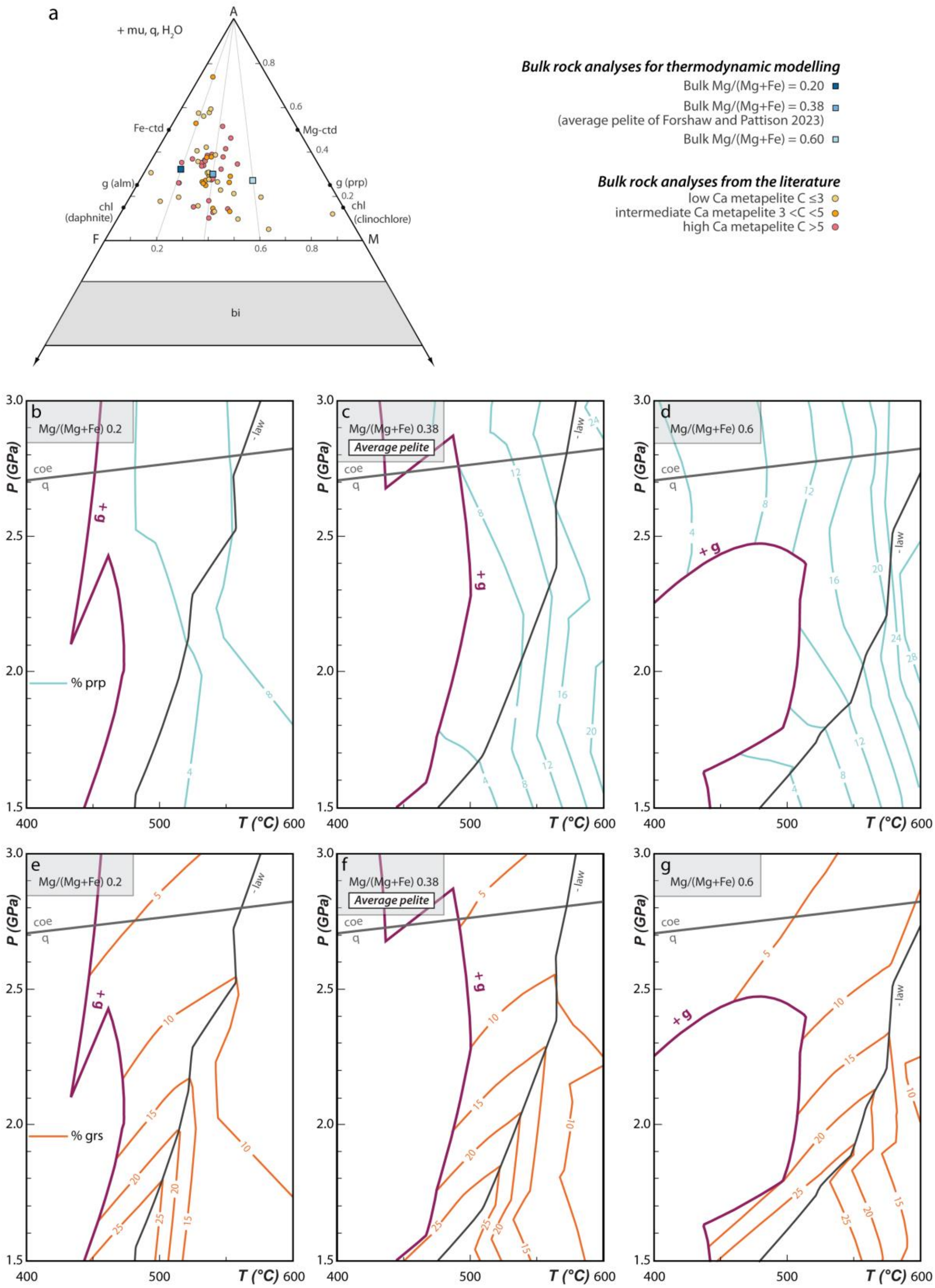

Fig. S21: (**a)** AFM diagram showing the bulk-rock compositions of the metapelites taken from the literature (see caption of Fig. 15 for details) projected from muscovite, quartz, and H_2O. The bulk rock compositions used for thermodynamic modelling are reported as squares. **(b,c,d,e,f,g)** *P*–*T* diagrams displaying (for three bulk rock compositions, plotted as squares in the AFM diagram above) the garnet-in and lawsonite-out lines, and the isopleths for pyrope content **(b,c,d)** and grossular content **(e,f,g)** in garnet. Note that the change of bulk rock chemistry has a significant effect on the location of the garnet-in ad lawsonite-out lines, and on the location of the pyrope isopleths.

References

Beyssac O, Goffé B, Chopin C, Rouzaud JN (2002) Raman spectra of carbonaceous material in metasediments: a new geothermometer. J Metamorph Geol 20:859–871

Beyssac O, Goffé B, Petitet JP, Froigneux E, Moreau M, Rouzaud JN (2003) On the characterization of disordered and heterogeneous carbonaceous materials using Raman spectroscopy. Spectrochim Acta A 59:2267–2276

de Capitani C, Brown TH (1987) The computation of chemical equilibrium in complex systems containing non-ideal solutions. Geochim Cosmochim Acta, 51:2639–2652

de Capitani C, Petrakakis K (2010) The computation of equilibrium assemblage diagrams with Theriak/Domino software. Amer Miner 95:1006–1016

Forshaw JB and Pattison DRM (2023) Major-element geochemistry of pelites. Geology 51:39–43

Green, ECR, White, RW, Diener, JFA, Powell, R., Holland, TJB., Palin, RM (2016). Activity–composition relations for the calculation of partial melting equilibria in metabasic rocks. J Metamorph Geol, 34, 845–869.

Holland, TJB, Powell, R (2011) An improved and extended internally consistent thermodynamic dataset for phases of petrological interest, involving a new equation of state for solids. J Metamorph Geol 29:333–383

Holland TJB Powell R (2003) Activity–composition relations for phases in petrological calculations: an asymmetric multicomponent formulation. Contrib Mineral Petrol 145:492–501

Manzotti P, Schiavi F, Nosenzo F, Pitra P, Ballèvre M (2022). A journey towards the forbidden zone: a new, cold, *UHP* unit in the Dora-Maira Massif (Western Alps). Contrib Mineral Petrol, 177:59.

Nosenzo F, Manzotti P, Robyr M (2023) H_2O budget and metamorphic re-equilibration in polycyclic rocks as recorded by garnet textures and chemistry. Lithos, 452–453, 107230

Pouchou JL, Pichoir F (1985) “PAP” $\phi(\rho Z)$ procedure for improved quantitative microanalysis. In: Armstrong JT (ed) Microbeam Analysis. San Francisco Press, San Francisco, CA, pp 104–106

Rasband W 1997. ImageJ. In: U.S. National Institutes of Health. U.S. National Institutes of Health. http://imageJ.nih.gov.

Wei CJ Powell R (2004) Calculated phase relations in high-pressure metapelites in the system NKFMASH (Na_2O–K_2O–FeO–MgO–Al_2O_3–SiO_2–H_2O). J Petrol 45:183–202

White RW, Powell R, Holland TJB, Worley BA (2000) The effect of TiO_2 and Fe_2O_3 on metapelitic assemblages at greenschist and amphibolite facies conditions: mineral equilibria calculations in the system K_2O-FeO-MgO-Al_2O_3-SiO_2-H_2O-TiO_2-Fe_2O_3. J Metamorph Geol 18:497–511

White RW, Powell R, Holland TJB, Worley B (2000) The effect of TiO_2 and Fe_2O_3 on metapelitic assemblages at greenschist and amphibolite facies conditions: mineral equilibria calculations in the system K_2O–FeO–MgO–Al_2O_3–SiO_2–H_2O–TiO_2–Fe_2O_3. J Metamorph Geol 18:497–511

White RW, Powell R, Clarke GL (2002) The interpretation of reaction textures in Fe-rich metapelitic granulites of the Musgrave Block, central Australia: constraints from mineral equilibria calculations in the system K_2O–FeO–MgO–Al_2O_3–SiO_2–H_2O–TiO_2–Fe_2O_3. J Metamorph Geol 20:41–55

White RW, Powell R, Johnson TE (2014a) The effect of Mn on mineral stability in metapelites revisited: new a–x relations for manganese-bearing minerals. J Metamorph Geol 32:809–828

White RW, Powell R, Holland TJB, Johnson TE, Green ECR (2014b) New mineral activity–composition relations for thermodynamic calculations in metapelitic systems. J Metamorph Geol 32:261–286